HHS Public Access

Author manuscript

Nat Cell Biol. Author manuscript; available in PMC 2012 April 27.

Published in final edited form as:

Nat Cell Biol. 2010 September ; 12(9): 902–908. doi:10.1038/ncb2094.

Coupling between clathrin-dependent endocytic budding and F-BAR-dependent tubulation in a cell-free system

Min Wu[1,2,4], **Bo Huang**[1,5,*], **Morven Graham**[2], **Andrea Raimondi**[1,2,4], **John E. Heuser**[7], **Xiaowei Zhuang**[1,5,6], and **Pietro De Camilli**[1,2,3,4,†]

[1]Howard Hughes Medical Institute; Neurodegeneration and Repair, Yale University School of Medicine, New Haven, CT 06520, USA

[2]Department of Cell Biology, Neurodegeneration and Repair, Yale University School of Medicine, New Haven, CT 06520, USA

[3]Department of Neurobiology, Neurodegeneration and Repair, Yale University School of Medicine, New Haven, CT 06520, USA

[4]Program in Cellular Neuroscience, Neurodegeneration and Repair, Yale University School of Medicine, New Haven, CT 06520, USA

[5]Department of Chemistry and Chemical Biology, Harvard University, Cambridge MA 02138, USA

[6]Department of Physics, Harvard University, Cambridge MA 02138, USA

[7]Department of Cell Biology and Physiology, Washington University School of Medicine, 660 South Euclid Avenue, St. Louis, MO 63110, USA

Abstract

Cell-free reconstitution of membrane traffic reactions and the morphological characterization of membrane intermediates that accumulate under these conditions have helped elucidate the physical and molecular mechanisms involved in membrane transport[1–3]. Towards an improved understanding of endocytosis we have reconstituted vesicle budding and fission from isolated plasma membrane sheets and imaged these events. Electron and fluorescence microscopy, including sub-diffraction-limit imaging by stochastic optical reconstruction microscopy (STORM) [4–6], revealed F-BAR (FBP17) domain coated tubules nucleated by clathrin-coated buds when fission was blocked (presence of GTPγS). Triggering fission by replacement of GTPγS with GTP led not only to separation of clathrin-coated buds, but also to vesicle formation by fragmentation of the tubules. These results suggest a functional link between FBP17 dependent

†Correspondence should be addressed to P.D.C.. pietro.decamilli@yale.edu.

*Present address: Dept of Pharmaceutical Chemistry, Dept of Biochemistry and Biophysics, University of California, San Francisco, CA 94158, USA

Author Contributions

M.W. and P.D.C. designed experiments and wrote the manuscript. M.W. performed experiments. Experimental work was also contributed by B.H. (STORM), J.E.H. (EM), A.R. (EM) and M.G. (EM). B.H. and X.Z. also contributed to discussion and manuscript preparation.

Competing Financial Interests

The authors declare no competing financial interests.

membrane tubulation and clathrin-dependent budding. They also show that clathrin spatially directs plasma membrane invaginations that lead to the generation of endocytic vesicles larger than those enclosed by the coat.

To gain new insight into mechanisms of endocytosis we developed a cell-free system suitable for monitoring the formation and progression of endocytic intermediates live at high resolution. Glass-attached plasma membrane sheets, left behind by sonication of fibroblasts grown on poly-d-lysine coated coverslips, were used as templates to reconstitute cytosol-dependent membrane budding. Sheets were visualized by fluorescence microscopy either by using cells expressing plasma membrane targeted GFP (PM-GFP) or by a brief incubation with the lipid dye Bodipy-Texas Red Ceramide (BTR) after lysis.

Sheets kept in cytosolic buffer revealed a diffuse and rather homogeneous fluorescence, with only a few sparse puncta (Fig 1a). Incubation with brain cytosol, ATP and non-hydrolyzable GTP analog GTPγS at 37°C induced, within minutes, the appearance of numerous fluorescence spots (Fig 1a, Supplemental Movie 1). Concomitant reduction in the glass-contact area of the sheets suggested that the spots represented membrane invaginations (Supplemental Fig 1). Approximately 15–32% of the total membrane area was sequestered into these membrane puncta during a 15 min incubation (Supplemental Figure 1).

When the same experiment was performed in the presence of GTP rather than GTPγS, few fluorescent spots can be observed at the end of a 15 min incubation (see Figure 3d), and a correspondingly smaller shrinkage of the membrane, less than 5%, was observed (Supplemental Figure 1). No appearances of puncta or shrinkage of the membrane occurred when sheets were incubated at 37°C with nucleotides but no cytosol.

To test if these fluorescent puncta were related to clathrin-coated pits, cytosol was supplemented with Alexa555-labeled clathrin. A near complete coincidence between fluorescent membrane puncta and clathrin was observed (Fig 1b). These membrane puncta also incorporated classical coated pit cargo, as shown by using membrane sheets derived from cells expressing one such cargo, pHluorin-tagged transferrin receptor (Fig 1b). Transferrin receptors became significantly more clustered after incubation with cytosol, ATP and GTPγS (Fig 1c, Supplemental Movie 2), with a corresponding reduction of fluorescence in the remaining portion of the sheets (Supplemental Figure 2). Furthermore, sites of transferrin receptor clustering colocalized completely with clathrin puncta (Fig 1b), indicating that they are sites of clathrin-coated pit nucleation.

To determine the ultrastructure of plasma membrane invaginations, three-dimensional stochastic optical reconstruction microscopy (3D-STORM) and electron microscopy (EM) were performed. 3D-STORM is a super-resolution fluorescence microscopy technique with spatial resolution of 20 nm in the x/y direction and 50nm in the z direction[6]. For this technique, PM-GFP labeled sheets were incubated with cytosol, ATP and GTPγS for 15 min, then fixed, labeled with antibodies directed against GFP and secondary antibodies conjugated with the photoswitchable dye pair Alexa405-Cy5. Reconstructed STORM images shows that the fluorescence membrane puncta observed by conventional

fluorescence microscopy were in fact highly elongated structures perpendicular to the surface (Fig 1d, Supplemental Movie 3).

Thin section EM as well as deep etch EM of platinum replica complemented these observations by revealing a massive presence of deep tubular plasma membrane invaginations (Fig 1e–g), which were always capped by one or several small clathrin-coated pits (diameter approx 50–70 nm). Occasionally, clathrin-coated pits were also localized along the tubules. The bulk of the tubules had a diameter of 57 ± 6 nm. They typically tapered sharply at their tips with a constriction at the boundary between the tubules and the coated pits (30–40 nm), and were often larger at their base next to the glass substrate (80–120 nm). Control plasma membranes incubated with cytosolic buffer alone revealed very little features other than some membrane undulation and occasional clathrin-coated pits that pre-existed the lysis. Cytosol plus ATP and GTP enhanced the number of clathrin-coated pits, but in both conditions, the dramatic tubulation was clearly absent (see Fig 3c). Note that in both of these conditions, PM-GFP fluorescence signal remained roughly homogenous (Fig 1a, Fig 3d). Thus, the invagination produced by a typical clathrin-coated pit is not sufficient to generate significantly higher membrane fluorescence signal relative to the surrounding membrane and under our experimental conditions fluorescent membrane puncta are in fact reporter of deep membrane invaginations.

To gain molecular insight into the nature of the tubules, we explored the potential presence of tubulating proteins with putative roles in endocytosis on these structures. Addition of fluorescently labeled dynamin [7], endophilin (a BAR protein) [8], and FBP17 (a F-BAR protein of the FBP17/CIP4/Toca1 family) [9–11] to the cytosol demonstrated that all these proteins were recruited to the sites of membrane invagination (Fig 2a, Supplemental Figure 3). However, although these proteins were localized to the same puncta in the *x*, *y* dimension, close examination in *z* stacks revealed segregation of these proteins along the axial direction of the tubules (Supplemental Figure 3). Dynamin precisely colocalized with endophilin both in the *x*, *y* dimension and in the *z* dimension. In contrast, dynamin and endophilin overlapped only partially with FBP17 in the *z* direction, being concentrated at the tip of the tubules.

Stacked 3D-STORM images of membrane invaginations labeled for clathrin (clathrin heavy chain directly labeled with Alexa 405-Cy5) and FBP17 (immunostained with Cy3-Cy5 labeled secondary antibodies) further demonstrated that FBP17 was present along the entire length of the large tubules (Fig 2b, c), while dynamin (directly labeled with Alexa 405-Cy5) was localized to the neck between the coated pit and the FBP17 coated tubules (Fig 2b). Accordingly, immunogold labeling of *en face* thin section revealed that FBP17 was localized on the wide portions of the tubules. These tubules had diameters between 50 nm and 120 nm (Fig 2d), the same size range of tubules generated by FBP17 when overexpressed in cells or incubated in vitro with liposomes[10, 12]. Dynamin localized exclusively to the narrow tubular necks linking wide tubules to the clathrin-coated buds (Fig 2d). The diameters of these neck regions are 35 ± 5 nm, consistent with the diameter of dynamin or endophilin coated tubules[13, 14].

We next analyzed the temporal sequence of clathrin recruitment and tubule elongation. To this aim, the distance between the clathrin signal and PM-GFP labeled basal membrane was imaged by two-color 3D-STORM at different time points after cytosol and nucleotides were added. Formation of clathrin-coated pits had already occurred at 5 min, with 2.1 ± 0.3 pits per μm^2 (Fig 3a, 3b, only the clathrin signals are displayed). At this time they were located close to the basal membrane, with an average distance of 90 ± 61 nm (Fig 3a, Supplemental Figure 4). At 15 min, they had risen to an average distance of 371 ± 204 nm from the basal membrane with 2.0 ± 0.3 pits per μm^2 (Fig 3a, Supplemental Figure 4). Thin section EM confirmed the assembly of clathrin-coated pits and their location next to the bottom surface at 5min (Fig 3c). Thus, under these cell free conditions, the recruitment of clathrin precedes tubule growth, suggesting that clathrin is needed for spatially guiding tubular growth.

When antibodies that block clathrin polymerization were included in the cytosol, membrane sheets remained roughly flat, indicating a lack of tubulation (Fig 3d). This was further confirmed by EM (Fig 3c). The absence of deep invaginations, despite the presence of abundant tubulating proteins in the cytosol, suggests that formation of clathrin-coated pits is not only needed to spatially direct tubular growth, but also to trigger tubular growth itself. Preincubation of cytosol with anti-FBP17 antibodies also strongly inhibited plasma membrane tubulating activity (Fig 3c, 3d), consistent with a strong presence of this protein in the wide tubular portion. In contrast, antibodies directed against dynamin did not prevent membrane tubulation, as indicated by the accumulation of fluorescence membrane puncta (Figure 3d).

In the presence of latrunculin B (125 μM), which blocks actin polymerization, clathrin-coated pits still accumulated on the membrane sheets (2.3 ± 0.2 pits per μm^2) as in the absence of the drug, but they remained close to the basal membrane with an average distance of about 79 ± 39 nm (Fig 3a, Supplemental Figure 4). Accordingly, EM demonstrated absence of the tubules under these conditions (Fig 3c). Many endocytic proteins, including proteins with robust tubulating activity such as FBP17, are intimately linked to actin polymerization[11, 15–16]. These results suggest that a synergistic action of actin and tubulating proteins is required for the formation of tubular invaginations in response to clathrin-coated pits nucleation. Similar results were recently reported in a system involving clathrin-dependent formation of tubular intermediates on giant unilamellar liposomes[17]. Interestingly, addition of latrunculin B (125 μM) to the membrane sheets after tubules have already formed led to loss of the actin cytoskeleton while tubules persisted (Supplemental Figure 5a–b). This observation suggests that, during tubulation, the action of actin facilitates the assembly of a stabilizing F-BAR domain-containing scaffold around the tubules. Intermolecular interactions within such scaffold may then contribute[12], at least in part, to tubule stability after actin disassembly, as supported by the slow turn over rate of FBP17 on the tubules revealed by FRAP (Supplemental Figure 5c–d).

Importantly, under all conditions where clathrin-coated pits assembled but wide tubules were absent, including in the presence of anti-FBP17 antibodies, the neck of clathrin-coated pits were constricted to a diameter below that of the large tubules (Fig 3c). Thus, neck constriction and wide tubular growth are likely two independently regulated processes, with the latter more dependent on FBP17.

Finally, to determine whether fission could occur in our cell free system, and whether tubular invaginations are important for this reaction, we monitored by fluorescence the appearance of free vesicles formed from PM-GFP labeled membrane sheets and their recovery on Sepharose beads coated with anti-GFP antibodies. Generation of free vesicles was virtually absent in the single incubation with cytosol, ATP plus GTPγS or GTP (Fig 4b). However, when cytosol plus ATP and GTP were added to the intermediates generated by a first incubation with cytosol, ATP and GTPγS, a large number of free vesicles was observed within minutes in the medium (Fig 4a, 4b, Supplemental Movie 4). These newly formed vesicles could be captured with minimal mechanical perturbation by beads coated with anti-GFP antibodies added together with the second incubation mixture (Fig 4c), but not by control beads devoid of specific antibodies (Supplemental Figure 6). PM-GFP puncta on the beads precisely colocalized with the fluorescent membrane marker BTR (Fig 4c, supplemental movie 5), confirming their membrane nature.

Thin section EM of the material recovered on the beads demonstrated the presence of small 40–70 nm coated and uncoated vesicles, as well as of larger vesicles of 100 to 400 nm (Fig 4d). A corresponding loss of tubular invaginations replaced by vesicular structures was observed on the membrane sheets (Fig 4e). These findings demonstrate the occurrence of fission and suggest that both clathrin-coated pits and tubular regions serve as precursors of free vesicles, with the small vesicles likely derived from the coated pits and the large vesicles likely arising from the large tubular region. No free vesicles were observed when GTPγS or latrunculin B were included in both incubations (Fig 4a, 4b). Antibodies directed against FBP17 did not completely abolish, but significantly inhibited vesicle formation when added to either incubation (Fig 4b).

Collectively, our results provide a striking demonstration of the hypothesis that membrane tubulation factors present in the cytosol are linked to endocytosis. FBP17 is one such factor, thus supporting an endocytic function of the FBP17/CIP4/Toca family, as previously suggested by functional[10, 11, 18] and genetic studies[19]. Our results further reveal a robust relation between clathrin-coated pits and FBP17-mediated tubulation. FBP17 was reported to be recruited to clathrin-coated pits in living fibroblasts[18]. The shallow curvature of the membrane binding surface of its F-BAR domain led to the hypothesis that FBP17 and other members of the FBP17/CIP4/Toca1 family may function prior to the final constriction of the pits[18], a process likely regulated by BAR domain proteins with a sharper curvature, such as amphiphysin[20], endophilin[8, 21] and SNX9[22]. An even earlier action was recently demonstrated for another F-BAR domain containing protein, FCHo[23]. FCHo is recruited prior to clathrin assembly and dissociates from clathrin coated pits as they mature, and thus was proposed to nucleate them[23]. This function is unlikely to be generally applicable to other F-BAR proteins since it is the C-terminal region of FCHo, the μ homology domain, that has a key role in its clathrin coated pits localization. F-BAR proteins of the FBP17/CIP4/Toca1 family, which contain a C-terminal SH3 domain instead of the μHD domain, are recruited later to clathrin coated pits[18, 23]. Importantly, FBP17 is not an essential component of clathrin coated pits in vivo, since it is not recruited to every clathrin coated pits in non-neuronal cells[23] and the triple knockdown of FBP17/CIP4/Toca1 only has partial inhibitory effect in transferrin uptake[10]. Our findings are consistent with a scenario according to which FBP17 mediated tubulation acts after (or in parallel with) the maturation of the pits and

independently contributes to membrane dynamics at the endocytic site, for example by regulating the extent of membrane internalized (Fig 5).

As in the case of all cell-free systems, the system that we have described does not precisely recapitulate conditions occurring in a living cell. Yet, it involves a natural plasma membrane template and cytosol, and thus closely mimics the physiological environment. Hence, the coordination of clathrin mediated budding with the formation of F-BAR domain coated tubules observed in this work likely reflects physiologically relevant phenomena. In live cells, membrane tubulation is expected to be antagonized by membrane tension[24, 25]. Membrane sheets prepared here represent a lower tension membrane template and may thus facilitate the production of tubular intermediates by FBP17, which may act as a tension sensor. The prominence of such tubules will be further enhanced by a defect in fission activity. For example, elongated tubular intermediates capped by clathrin-coated pits with similar diameter to those described in this study have been observed in garland cells of *shibire*, a temperature sensitive mutant of dynamin[26]. Nevertheless, similar intermediates have also been seen in wild type cells[27, 28]. Appearance of such intermediates may result from a transient shift in balance between tubulation and fission activity due to regulatory mechanisms in vivo. In addition, unconventional roles of clathrin in endocytosis have been described[29], and in some cases the endocytic reaction results in the internalization of plasma membrane fragments that are larger than the vesicle scaffolded by the clathrin coat itself[30]. Taken together, our study provide strong support to the importance of F-BAR-dependent tubular endocytic intermediates in endocytosis and reveals new endocytic intermediates that likely correspond to physiologically occurring stage of endocytosis. The generation of large membrane fragments from the plasma membrane sheets can be considered a form of clathrin dependent bulk endocytosis. Thus, our study also demonstrates the possibility of using a cell free system to study this still mechanistically elusive endocytic reaction.

Methods

Reagents

Antibodies to clathrin heavy chain (X22, Affinity Bioreagents, Golden, CO), dynamin (clone 41, BD transduction), GFP (rabbit IgG, Invitrogen) and gold conjugated (12nm or 6nm particles, Jackson ImmunoResearch) anti-rabbit antibodies were purchased commercially. Polyclonal antibodies to dynamin (DG1) for immunogold localization were generated by our lab and described previously[31]. Polyclonal antibodies to FBP17 for immunogold and STORM localization were generated by our lab and described previously[10]. Fluorescent lipid BODIPY TR ceramide (BTR) was purchased from Invitrogen. Rhodamine skeletal muscle actin was purchased from Cytoskselton, Inc. All other chemicals were from Sigma.

Cytosol

Adult mouse brains were homogenized in breaking buffer [25mM Tris(pH8.0), 500mM KCl, 250mM sucrose, 2mM EGTA, 1mM DTT] in the presence of a protease inhibitor cocktail (Roche). The lysate was centrifuged at 160,000g for 2 hours and the resulting supernatant was desalted on PD-10 (Amersham Biosciences) at room temperature into

cytosolic buffer [25mM Hepes, pH 7.4, 120mM potassium glutamate, 20mM potassium chloride, 2.5mM magnesium acetate, 5mM EGTA]. Aliquots of cytosol were frozen in liquid nitrogen and stored at −80°C for up to two months.

Purified proteins and their conjugation to fluorophores

The following commercial fluorophores were used in protein conjugations: Alexa 488 maleimide (Invitrogen A10254), Alexa 555 maleimide (Invitrogen A20346), Alexa 594 maleimide (Invitrogen A10256). Covalently linked activator-reporter pairs Alexa 405-Cy5 maleimide has been prepared as described previously[32].

Clathrin was purified from bovine brains according to described previously[33]. To conjugate clathrin with fluorescent dyes, clathrin was reacted with the dyes (Alexa 405-Cy5 or Alexa 555 maleimide, dye protein molar ratio 8) at room temperature for 30 min. One round of polymerization and depolymerization was done to remove non-functional clathrin or aggregates. Briefly, the reaction product was dialyzed into polymerization buffer [40mM NaMES (pH6.5), 3mM $CaCl_2$, 0.5mM $MgCl_2$, 1mM EGTA, 1mM DTT] overnight at 4°C. The solution was centrifuged at 150,000g for 1h and the resulting pellet was resuspended into depolymerization buffer [20mM TrisHCl (pH7.8), 1mM EDTA] and dialyzed into the same buffer overnight at 4°C. After centrifugation at 150,000g for 1h, the supernatant was collected and dialyzed into storage buffer [20mM Hepes (pH7.4), 120mM NaCl, 1mM DTT].

Dynamin was purified from rat brains and conjugated with fluorescent dyes (Alexa 488 maleimide, Alexa405-Cy5 maleimide) as described[34]. FBP17 was purified as GST fusion protein as described[10]. After cleavage of the GST tag, FBP17 was conjugated to Alexa 488 maleimide (Invitrogen A10254) by reacting with the dye (dye protein molar ratio 4) at room temperature for 30min. The final product was dialyzed into high salt storage buffer [20mM Hepes (pH7.4), 300mM NaCl, 1mM DTT].

Membrane sheets

PTK2 cells were maintained at 37°C in 10% CO2 in Minimum Essential Eagle Medium (Invitrogen) supplemented with 10% (v/v) fetal bovine serum, 100 μg/ml penicillin/streptomycin. PTK2 cells stably expressing PM-GFP[35], transferrin receptor-phluorin[36] were maintained with 0.5mg/ml G418. To prepare membrane sheets[37–39], cells were grown for 24–48 hours until confluency in MatTek dishes (MatTek Corporation, Ashland, MA) that had been coated with 20 μg/ml poly-d-lysine for 30min and washed overnight. They were sheared in ice-cold cytosolic buffer [25mM Hepes, pH 7.4, 120mM potassium glutamate, 20mM potassium chloride, 2.5mM magnesium acetate, 5mM EGTA] with 1mM DTT by a brief pulse of sonication (~1s) using a cell disruptor (VirTis Ultrasonics, NY) set at 15–17% of output power with a 1/8-inch microprobe positioned at ~15mm above the dish. After shearing, membrane sheets were rinsed in cytosolic buffer and used for the in vitro assay within twenty minutes. When a fluorescent lipid marker was used to visualize the membrane, membrane sheets were incubated with 5 μM BTR at 37°C for 5min and rinsed to remove excess dyes.

In vitro assay

membrane sheets were incubated at 37°C with cytosol and nucleotides as indicated. The final concentration of cytosol and nucleotides was as follows: cytosol: 4mg/ml; ATP: 1.5 mM; GTPγS: 150 μM; GTP: 1.6 mM; Samples containing ATP were supplemented with an ATP-regenerating system consisting of 16.7 mM creatine phosphate and 16.7 U/mL creatine phosphokinase[20]. Samples containing GTP were supplemented with a GTP-regenerating system consisting of 1mM phosphopyruvate and 20 U/ml pyruvate kinase. Fluorescent proteins added to the cytosol were used at the following concentrations: clathrin: 500 nM; dynamin: 125 nM; FBP17: 50–250 nM. When indicated, cytosol was preincubated with anti-clathrin (0.5 mg/ml), anti-dynamin (50 μg/ml) or anti-FBP17 (20 μg/ml) at 4°C for 1–2h. Heat denatured antibodies were used as negative control. In real time imaging, an oxygen scavenging system [4.5mg/ml glucose, 1.25 μM glucose oxidase, 140 nM catalase, 71.5 mM 2-mercaptoethanol] was included. For two-step fission assay, membrane sheets were incubated with first dose of cytosolic mixture for 15–20 min, washed with cytosolic buffer and incubated with second dose of cytosolic mixture. For Immunocapture of the fissioned vesicles, protein A Sepharose CL-4B beads (GE Healthcare, Piscataway, NJ) were coated with anti-GFP (0.4 mg/ml) at 4°C for 1h, washed in cytosolic buffer, and added together with second dose of cytosolic mixture at a volume ratio of 1:10.

Fluorescence microscopy and image analysis

Epifluorescence imaging was done using a Leica DMI6000 inverted microscopy equipped with CCD camera (Coolsnap HQ, company) and temperature controlled chamber. A mercury lamp (EXFO X-Cite 120) or a xenon arc lamp (Lambda DG-4) was used as light source. All images were acquired through either 63× oil (NA1.3, PL APO) or 100x oil (NA1.4, PL APO) objectives and the following filter combinations: Ex: BP 470/40; Dich: 500; Em: BP 525/50 for green; Ex: BP 546/12 Dich: 560; Em: BP 605/75 for red; Ex: BP 565/55; Dich: 600; Em: BP 650/75 for far red. Metamorph (Universal Imaging, Downington, PA) was used to acquire either single color image or sequential two color images using binning 2.

Real time fission assay and FRAP experiment were performed on an UltraVIEW VoX spinning disc confocal (SDC) microscope (Perkin Elmer, Waltham, MA) equipped with Perfect Focus, temperature controlled stage, EMCCD camera (Hamamatsu C9100-50) and controlled by Volocity software (Improvision). All images were acquired through a 60× or 100× oil objective (NA 1.4, CFI Plan Apo VC). Green fluorescence was excited with a 488 nm/50 mW diode laser and collected by a BP 527/55 filter. Red fluorescence was excited with a 561 nm/50 mW diode laser and collected by a BP 615/70 filter. Two color images were acquired sequentially. For Fluorescence recovery after photobleaching, a region of interest (50×50 pixels, 14 μm^2) was chosen on the sheet and the 488 nm/50 mW laser at 100% power was used to bleach this region for 100 cycles. Images were acquired by a 100× oil objective (NA 1.4, CFI Plan Apo VC) at 10 sec intervals and at least 10 frames were acquired before bleaching.

Quantification of fission events was done by counting fluorescence spots in SDC images using custom written algorithm in Matlab. Briefly, for each reaction, a 30 min movie

(usually 180 frames), including before and after adding GTP, was acquired at 20 μm above the surface. Median filter was applied to each frame of the image series and local background was subtracted. Vesicles were identified as pixels with local maximum intensity above a fixed threshold. The identified particles were overlaid with original movie for visual inspection. The number of the vesicles per frame (1000×1000 pixels, 14,400 μm^2) was plotted against time and fifty frames with highest number of peaks were averaged to give the final number for this reaction. For each condition, three to eight independent experiments were performed.

Quantification of FRAP was done by calculating the average intensity of the bleached region, which was corrected with background (average intensity of a non-fluorescent region) and normalized with the average intensity of a neighboring fluorescent but non-bleached region to account for global intensity changes. The subsequent recovery curve was fitted with the Soumpasis equation

$$F(t)=A\cdot e^{-2T/t}\cdot(I_0(2T/t)+I_1(2T/t))+B$$

where I_0, I_1 are modified Bessel functions, A, B and T are free parameters that describe the increase in fluorescence intensity after recovery $F(\infty)$-$F(0)$, the fluorescence intensity immediately after bleaching $F(0)$ and the recovery time.

STORM

After the in vitro reaction, samples were rinsed and fixed in 4% paraformaldehyde, 0.1% glutaraldehyde and 5 μM phalloidin at room temperature for 20 min. In the case of immuno-staining, after incubation with primary (rabbit anti-FBP17: 1:200; rabbit anti-GFP 1:200) and secondary antibody (1:200) for 30 min, respectively, samples were fixed for additional 20 min. Imaging was done as described[6, 32]. Briefly, super-resolution images were acquired on an Olympus IX-71 inverted microscope equipped with a 100× NA 1.4 oil immersion objective. Three activation lasers and one imaging laser (CUBE 405-50C and Sapphire 460-10 from Coherent, GCL-200-L and RCL-200-656 from Crystalaser) are individually shuttered and illuminate the sample in wide-field high-incident-angle mode. A dichroic mirror (T660LPXR, Chorma) and an emission filter (ET705/70m, Chroma) allows the single-molecule photoactivation events to be captured by an EMCCD camera (Ixon DV897DCS-BV, Andor) through a cylindrical lens that creates an astigmatism for 3D localization. The reflected imaging laser from the bottom of the culture dish was redirected to a quadrant photodiode, providing the feedback signal to a piezo objective positioner (Nano F-100, Madcity Labs) to stabilize the focusing of the microscope. One STORM image consists of 1 to 3 *z*-slices acquired at focal plane positions separated by approximately 470 nm to cover the entire height of the sample, with 5000–10000 raw image frames recorded per slice. After correcting for the spherical aberration of refractive index mismatch between the coverglass and imaging buffer[32], each slice covers a *z* range of about 650 nm to 900 nm depending on the distance of the focal plane to the coverglass surface. Crosstalk between color channels was subtracted statistically.

Electron microscopy

Samples were fixed in 2.5% glutaraldehyde containing 1% tannic acid for 1 hour at room temperature, rinsed 3 times in cytosolic buffer, stained in 1% osmium tetroxide in phosphate buffer [100mM sodium phosphate, 50mM KCl, 5mM $MgCl_2$, pH6] for 1 hour, rinsed, en bloc stained in 2% uranyl acetate in maleate buffer [50mM, pH5.2] and rinsed again. Subsequently samples were dehydrated in an ethanol series and infiltrated using Epon812 resin and baked over night at 60°C. Sample containing resins were separated from the glass coverslip and the first few 60nm sections from each surface were cut using a Leica UltraCut UCT. Sections were lightly stained using 2% uranyl acetate and lead citrate and viewed on FEI Tencai Biotwin TEM at 80Kv spot size 1. Images were taken using Morada CCD and iTEM software (Olympus).

Immunogold

Samples were fixed in 4% paraformaldehyde, 0.1% glutaraldehyde and 5 μM phalloidin at room temperature for 15 min, rinsed, and blocked in 1% fish skin gelatin and 10% Normal Donkey Serum in PBS for 30 minutes. Coverslips were then incubated with the primary antibodies (rabbit anti-FBP17 1:10, or rabbit anti-dynamin 1:10) for 30 min. After rinsed in buffer for 15 minutes, they were incubated in secondary antibodies (12nm or 6nm directly conjugated gold anti-rabbit antibody) for 30 min. The samples were rinsed in PBS and then post fixed in 2.5% glutaraldehyde containing 1% tannic acid for 1 hour at room temperature, and processed as described above.

Deep Etch Electron Microscopy

Samples were fixed in 2% glutaraldehyde, 5 μM phalloidin at room temperature for 20 min and processed as described[40].

Supplementary Material

Refer to Web version on PubMed Central for supplementary material.

Acknowledgements

We thank Aurelien Roux and Yuxin Mao for advice and help, Lijun Liu, Frank Wilson and Christoph Rahner for critical technical assistance. This work was supported in part by the G. Harold and Leila Y. Mathers Charitable Foundation, the W.M. Keck Foundation and the National Institutes of Health grants (NS36251 and DK45735) to P.D.C. and National Institutes of Health grant (GM 068518) to X.Z. P.D.C. and X.Z. are Howard Hughes Medical Institute Investigators.

References

1. Moore M, Mahaffey D, Brodsky F, Anderson R. Assembly of clathrin-coated pits onto purified plasma membranes. Science. 1987; 236:558–563. [PubMed: 2883727]
2. Smythe E, Pypaert M, Lucocq J, Warren G. Formation of coated vesicles from coated pits in broken A431 cells. The Journal of Cell Biology. 1989; 108:843–853. [PubMed: 2564003]
3. Schmid SL, Smythe E. Stage-specific assays for coated pit formation and coated vesicle budding in vitro. The Journal of Cell Biology. 1991; 114:869–880. [PubMed: 1908470]
4. Rust MJ, Bates M, Zhuang X. Sub-diffraction-limit imaging by stochastic optical reconstruction microscopy (STORM). Nat Meth. 2006; 3:793–796.

5. Bates M, Huang B, Dempsey GT, Zhuang X. Multicolor Super-Resolution Imaging with Photo-Switchable Fluorescent Probes. Science. 2007; 317:1749–1753. [PubMed: 17702910]
6. Huang B, Wang W, Bates M, Zhuang X. Three-Dimensional Super-Resolution Imaging by Stochastic Optical Reconstruction Microscopy. Science. 2008; 319:810–813. [PubMed: 18174397]
7. Hinshaw JE. Dynamin and its role in membrane fission. Annual Review of Cell and Developmental Biology. 2000; 16:483–519.
8. Farsad K, et al. Generation of high curvature membranes mediated by direct endophilin bilayer interactions. Journal of Cell Biology. 2001; 155:193–200. [PubMed: 11604418]
9. Kamioka Y, et al. A Novel Dynamin-associating Molecule, Formin-binding Protein 17, Induces Tubular Membrane Invaginations and Participates in Endocytosis. Journal of Biological Chemistry. 2004; 279:40091–40099. [PubMed: 15252009]
10. Itoh T, et al. Dynamin and the Actin Cytoskeleton Cooperatively Regulate Plasma Membrane Invagination by BAR and F-BAR Proteins. Dev Cell. 2005; 9:791–804. [PubMed: 16326391]
11. Tsujita K, et al. Coordination between the actin cytoskeleton and membrane deformation by a novel membrane tubulation domain of PCH proteins is involved in endocytosis. J. Cell Biol. 2006; 172:269–279. [PubMed: 16418535]
12. Frost A, et al. Structural Basis of Membrane Invagination by F-BAR Domains. Cell. 2008; 132:807–817. [PubMed: 18329367]
13. Takei K, McPherson PS, Schmid SL, Camilli PD. Tubular membrane invaginations coated by dynamin rings are induced by GTP-[gamma]S in nerve terminals. Nature. 1995; 374:186–190. [PubMed: 7877693]
14. Ringstad N, et al. Endophilin/SH3p4 Is Required for the Transition from Early to Late Stages in Clathrin-Mediated Synaptic Vesicle Endocytosis. Neuron. 1999; 24:143–154. [PubMed: 10677033]
15. Ho H-YH, et al. Toca-1 Mediates Cdc42-Dependent Actin Nucleation by Activating the N-WASP-WIP Complex. Cell. 2004; 118:203–216. [PubMed: 15260990]
16. Takano K, Toyooka K, Suetsugu S. EFC/F-BAR proteins and the N-WASP-WIP complex induce membrane curvature-dependent actin polymerization. EMBO J. 2008; 27:2817–2828. [PubMed: 18923421]
17. Anitei M, et al. Protein complexes containing CYFIP/Sra/PIR121 coordinate Arf1 and Rac1 signalling during clathrin-AP-1-coated carrier biogenesis at the TGN. Nat Cell Biol. 2010; 12:330–340. [PubMed: 20228810]
18. Shimada A, et al. Curved EFC/F-BAR-Domain Dimers Are Joined End to End into a Filament for Membrane Invagination in Endocytosis. Cell. 2007; 129:761–772. [PubMed: 17512409]
19. Giuliani C, et al. Requirements for F-BAR Proteins TOCA-1 and TOCA-2 in Actin Dynamics and Membrane Trafficking during *Caenorhabditis elegans* Oocyte Growth and Embryonic Epidermal Morphogenesis. PLoS Genet. 2009; 5:e1000675. [PubMed: 19798448]
20. Takei K, Slepnev VI, Haucke V, De Camilli P. Functional partnership between amphiphysin and dynamin in clathrin-mediated endocytosis. Nat Cell Biol. 1999; 1:33–39. [PubMed: 10559861]
21. Ferguson S, et al. Coordinated Actions of Actin and BAR Proteins Upstream of Dynamin at Endocytic Clathrin-Coated Pits. Dev Cell. 2009; 17:811–822. [PubMed: 20059951]
22. Soulet F, Yarar D, Leonard M, Schmid SL. SNX9 Regulates Dynamin Assembly and Is Required for Efficient Clathrin-mediated Endocytosis. Mol. Biol. Cell. 2005; 16:2058–2067. [PubMed: 15703209]
23. Henne WM, et al. FCHo Proteins Are Nucleators of Clathrin-Mediated Endocytosis. Science. 2010; 328:1281–1284. [PubMed: 20448150]
24. Sheetz MP, Dai J. Modulation of membrane dynamics and cell motility by membrane tension. Trends in Cell Biology. 1996; 6:85–89. [PubMed: 15157483]
25. Zimmerberg J, Kozlov MM. How proteins produce cellular membrane curvature. Nat Rev Mol Cell Biol. 2006; 7:9–19. [PubMed: 16365634]
26. Kosaka T, Ikeda K. Reversible blockage of membrane retrieval and endocytosis in the garland cell of the temperature-sensitive mutant of Drosophila melanogaster, shibirets. J. Cell Biol. 1983; 97:499–507. [PubMed: 6411734]

27. Willingham M, et al. Receptor-mediated endocytosis in cultured fibroblasts: cryptic coated pits and the formation of receptosomes. J. Histochem. Cytochem. 1981; 29:1003–1013. [PubMed: 6169759]
28. He W, et al. FcRn-mediated antibody transport across epithelial cells revealed by electron tomography. Nature. 2008; 455:542–546. [PubMed: 18818657]
29. Veiga E, et al. Invasive and Adherent Bacterial Pathogens Co-Opt Host Clathrin for Infection. Cell Host & Microbe. 2007; 2:340–351. [PubMed: 18005755]
30. Cureton DK, Massol RH, Saffarian S, Kirchhausen TL, Whelan SPJ. Vesicular Stomatitis Virus Enters Cells through Vesicles Incompletely Coated with Clathrin That Depend upon Actin for Internalization. PLoS Pathog. 2009; 5:e1000394. [PubMed: 19390604]
31. Butler MH, et al. Amphiphysin II (SH3P9; BIN1), a Member of the Amphiphysin/Rvs Family, Is Concentrated in the Cortical Cytomatrix of Axon Initial Segments and Nodes of Ranvier in Brain and around T Tubules in Skeletal Muscle. J. Cell Biol. 1997; 137:1355–1367. [PubMed: 9182667]
32. Huang B, Jones SA, Brandenburg B, Zhuang X. Whole-cell 3D STORM reveals interactions between cellular structures with nanometer-scale resolution. Nat Meth. 2008; 5:1047–1052.
33. Campbell C, Squicciarini J, Shia M, Pilch PF, Fine RE. Identification of a protein kinase as an intrinsic component of rat liver coated vesicles. Biochemistry. 1984; 23:4420–4426. [PubMed: 6148963]
34. Roux A, Uyhazi K, Frost A, De Camilli P. GTP-dependent twisting of dynamin implicates constriction and tension in membrane fission. Nature. 2006; 441:528–531. [PubMed: 16648839]
35. Chen H, De Camilli P. The association of epsin with ubiquitinated cargo along the endocytic pathway is negatively regulated by its interaction with clathrin. Proceedings of the National Academy of Sciences. 2005; 102:2766–2771.
36. Merrifield CJ, Perrais D, Zenisek D. Coupling between Clathrin-Coated-Pit Invagination, Cortactin Recruitment, and Membrane Scission Observed in Live Cells. Cell. 2005; 121:593–606. [PubMed: 15907472]
37. Heuser J. The Production of 'Cell Cortices' for Light and Electron Microscopy. Traffic. 2000; 1:545–552. [PubMed: 11208142]
38. Lin H, Moore M, Sanan D, Anderson R. Reconstitution of clathrin-coated pit budding from plasma membranes. J. Cell Biol. 1991; 114:881–891. [PubMed: 1908471]
39. Holroyd P, Lang T, Wenzel D, De Camilli P, Jahn R. Imaging direct, dynamin-dependent recapture of fusing secretory granules on plasma membrane lawns from PC12 cells. Proceedings of the National Academy of Sciences. 2002; 99:16806–16811.
40. Heuser J. Effects of cytoplasmic acidification on clathrin lattice morphology. J. Cell Biol. 1989; 108:401–411. [PubMed: 2563729]

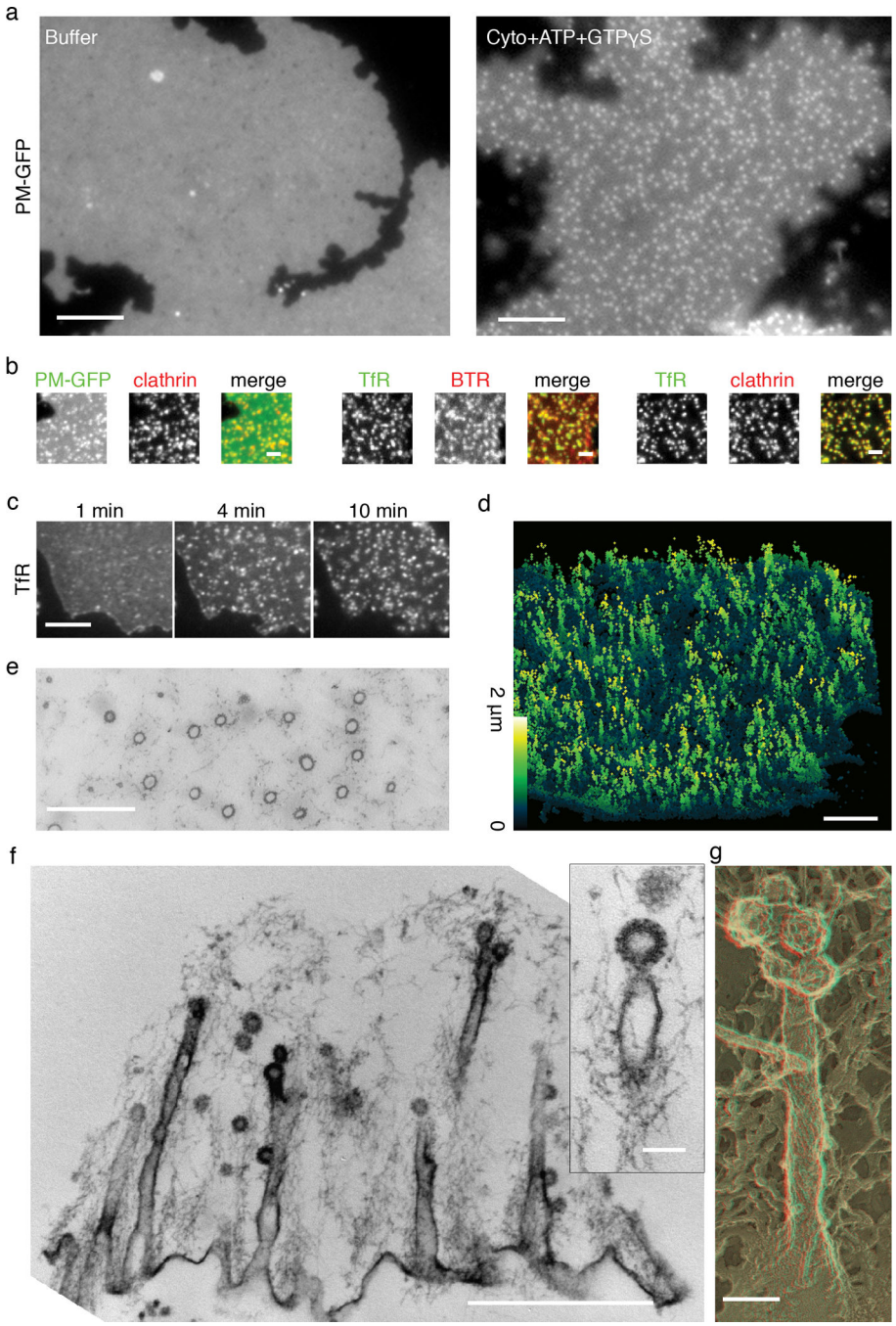

Figure 1.

Dramatic transformation of plasma membrane sheets induced by incubation with brain cytosol. (a) Plasma membrane sheets labeled with PM-GFP appear homogeneous without cytosol treatment but become punctate after 15 min incubation with cytosol (Cyto), ATP and GTPγS. Also see Supplemental Movie 1. (b) Membrane puncta that accumulate on plasma membrane sheets endogenously labeled by PM-GFP or exogenously labeled by fluorescent lipid marker BTR) colocalize with clathrin (Alexa 555 labeled clathrin heavy chain) or transferrin receptor-pHluorin (TfR) puncta. (c) Time sequence of transferrin receptor-

pHluorin clustering (see Supplemental Movie 2). (d) 3D-STORM reconstruction of the transformed plasma membrane. Membrane sheets labeled with PM-GFP were incubated with cytosol, ATP and GTPγS for 15 min, fixed and labeled with anti-GFP, followed by secondary antibody (see Supplemental Movie 3). Color of individual points in the image encodes distance from the substrate ranging from 0 to 2 μm. (e) Circular membrane profiles in *en face* thin sections demonstrating the tubular nature of the invaginations. (f) Thin section cut perpendicular to the substrate showing longitudinal view of the deep tubular structures that are connected with clathrin-coated pits via constricted necks. (g) EM of the platinum replica of quick-frozen deep-etched membrane sheet illustrating deep tubular extensions capped with multiple clathrin-coated pits. (e)–(g) were all incubated with cytosol, ATP and GTPγS for 15 min. Scale bars: 5 μm (a); 2 μm (b); 5 μm (c); 2 μm (d); 1 μm (e); 1 μm (f); 100 nm (f) insert and (g).

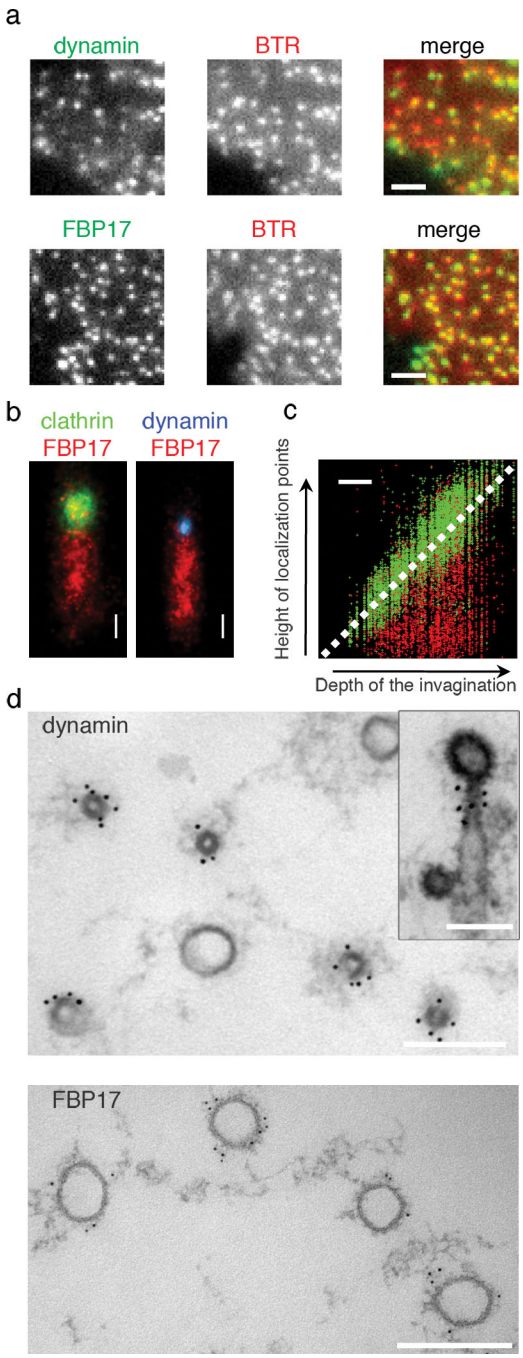

Figure 2.

Localization and axial segregation of dynamin and FBP17 along the tubular invaginations. (a) Alexa488 dynamin and Alexa 488 FBP17 were both recruited to the membrane invaginations as indicated by fluorescence lipid puncta (BTR). (b) Stacked 3D-STORM images of 59 membrane invaginations labeled by FBP17 (immunofluorescence with Cy3-Cy5 labeled secondary antibodies) and aligned according to the position of the coat region (Alexa 405-Cy5 labeled clathrin heavy chain), and of 96 membrane invaginations aligned according to the position of the constriction site where dynamin (Alexa 405-Cy5 labeled

dynamin) was localized. (c) The distribution of clathrin and FBP17 along the length of tubules as a function of the depth of invaginations. The *x*–*z* 3D-STORM images of 207 membrane invaginations labeled by FBP17 (immunofluorescence with Cy3/Cy5 labeled secondary antibodies) and clathrin (Alexa 405-Cy5 labeled clathrin heavy chain) were used to generate this scatter plot. Clathrin localization points follow the diagonal line as expected, whereas FBP17 points fill the space underneath the clathrin structure regardless of the depth of the invagination. (d) Immunogold localization of FBP17 and dynamin (polyclonal antibody DG1) on cross sections of the tubular invaginations. The top section captured a plane closer to the tip of the tubules. Inset shows a side view. All samples in Figure 2 were prepared by incubating membrane sheets with cytosol, ATP and GTPγS for 15min then fixed. Scale bars: 2 μm (a); 200 nm (b–d);

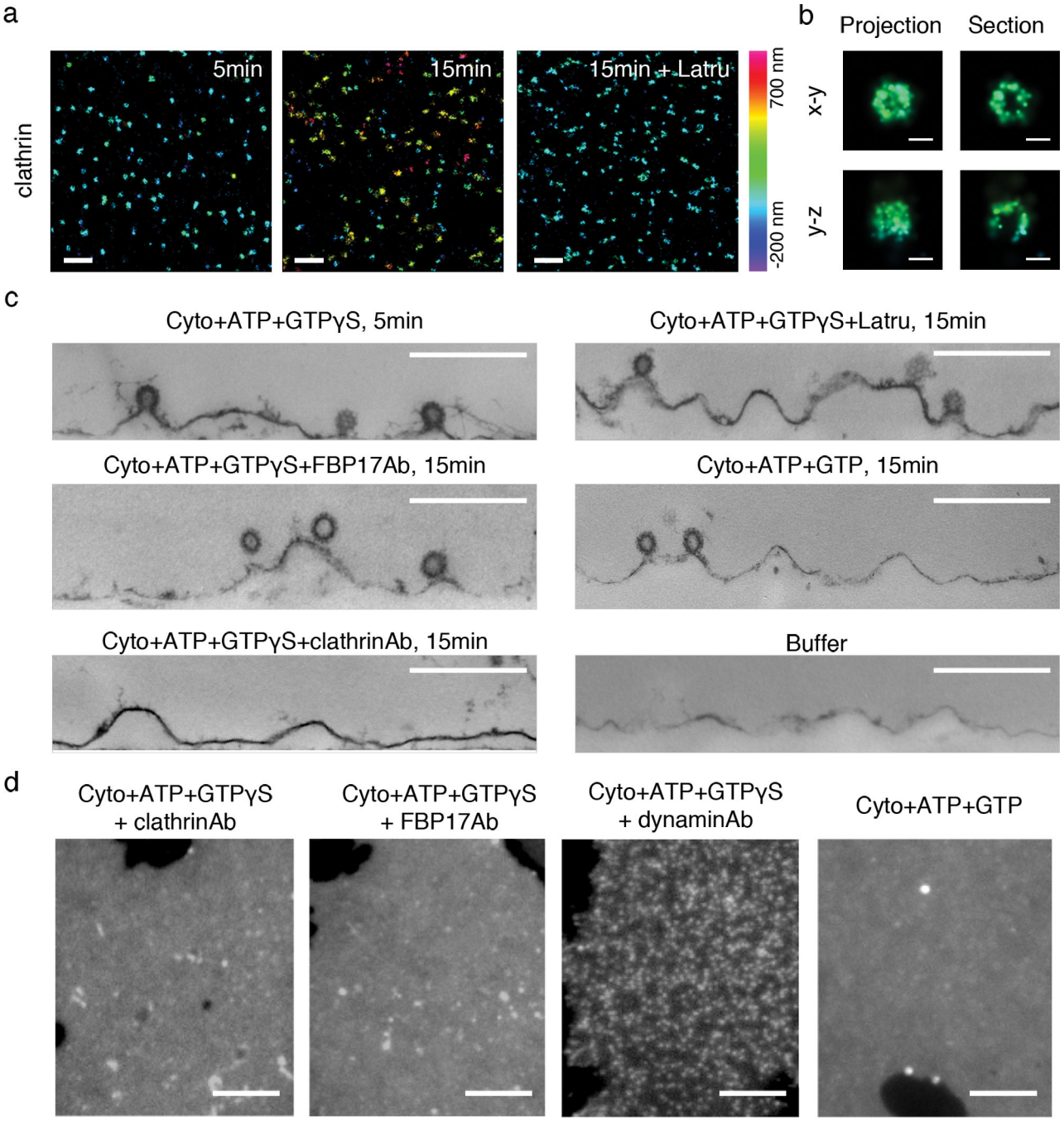

Figure 3.

Tubular invaginations require spatially coordinated action of clathrin, actin and FBP17. (a) 3D-STORM images of clathrin (Alexa 405-Cy5 labeled clathrin heavy chain) at different time points after incubation with cytosol, ATP plus GTPγS and in the absence or presence of latrunculin B (Latru). Two color 3D imaging was performed together with PM-GFP (not displayed here). (b) High-magnification view of 3D-STORM images of a single clathrin-coated pit. In the right panels, the horizontal and vertical projections of the 3D image of one clathrin structure display the half-spherical shape of the pit, whereas 50 nm thick cross

sections through the geometric center of the pit reveals its hollow inside (in both *x*–*y* and *y*–*z* views) and the opening at the bottom (only in *y*–*z* view), as expected for clathrin-coated pits. In both (a) and (b), color of individual points in the images encodes distance from the average height of the basal membrane sheet, ranging from -200 nm to 700 nm. (c) Thin section EM confirms the presence of clathrin-coated pits but a lack of tubulation at early point (5min) of incubation with cytosol, ATP plus GTPγS, or at later time point (15min) in the presence of latrunculin B, anti-FBP17 antibodies (FBP17Ab), or GTP instead of GTPγS. In the absence of cytosol or in the presence of anti-clathrin antibodies (clathrinAb), clathrin-coated pits are rare. (d) Fluorescence images of plasma membrane sheets (labeled by PM-GFP) after incubations as indicated. Scale bars: 1 μm (a); 100 nm (b); 500 nm (c); 5 μm (d).

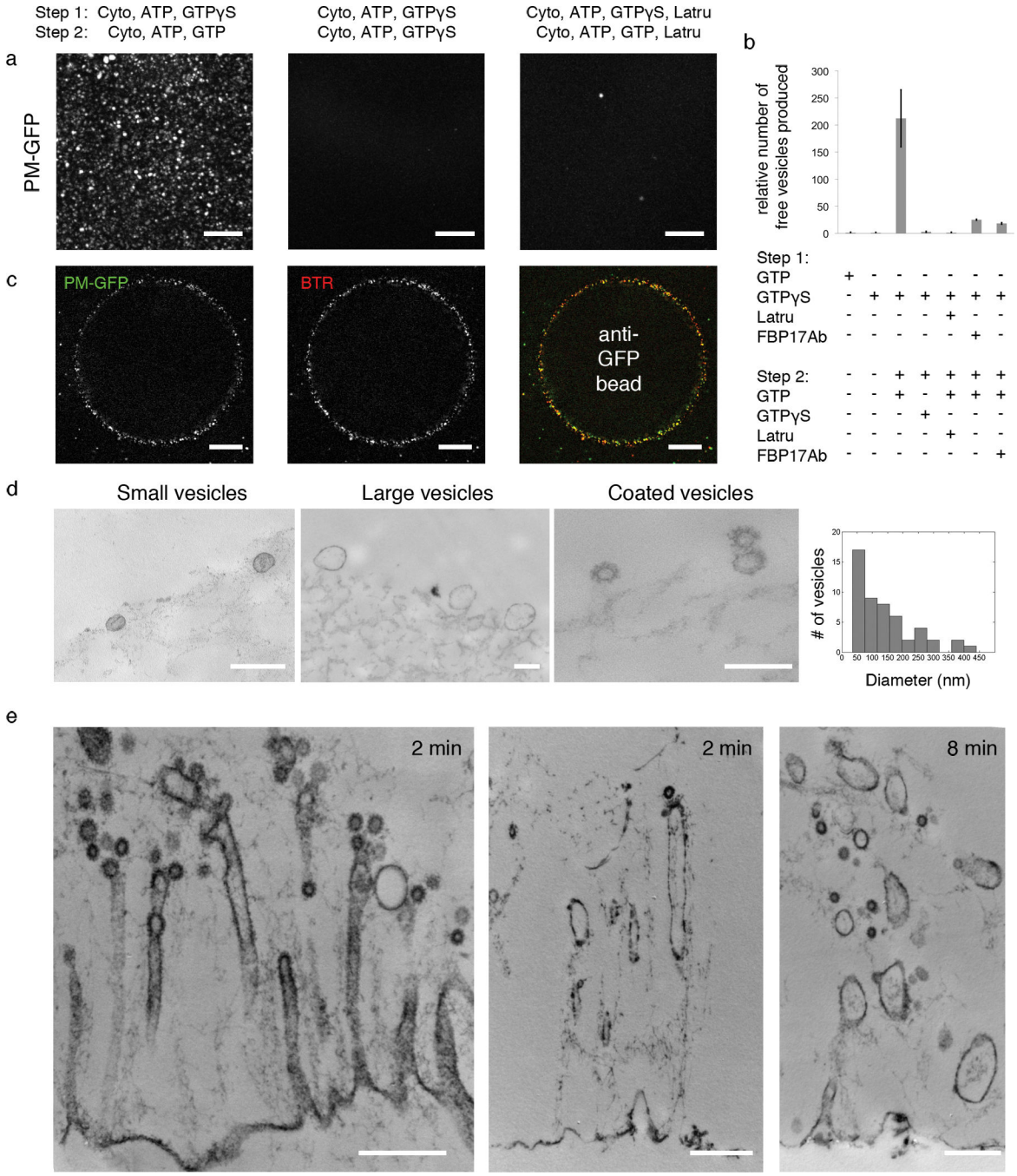

Figure 4.

Occurrence of membrane fission upon replacement of GTPγS with GTP. (a) Appearance of free vesicles (labeled by PM-GFP) in the medium in the presence of GTP, but not in the continued presence of GTPγS or latrunculin B. Each image is the maximum intensity projection of fifty frames by confocal microscopy. Also see Supplemental Movie 4. (b) Quantification of the number of free vesicles formed under various incubation conditions. The number for each condition was obtained by counting the average number of vesicles per frame (see Methods for details). Data represent means ± s.e.m. (n = 3–8 experiments for

each condition). (c) Immunocapture of vesicles (PM-GFP positive) on beads coated with anti-GFP antibodies and colocalization with a membrane marker (BTR) (see Supplemental Movie 5). (d) EM of bead-bound vesicles and distribution of their diameters. (e) EM of plasma membrane sheets at various time point after replacement of GTPγS with GTP. Scale bars: 10 μm (a); 20 μm (c); 200 nm (d); 500 nm (e).

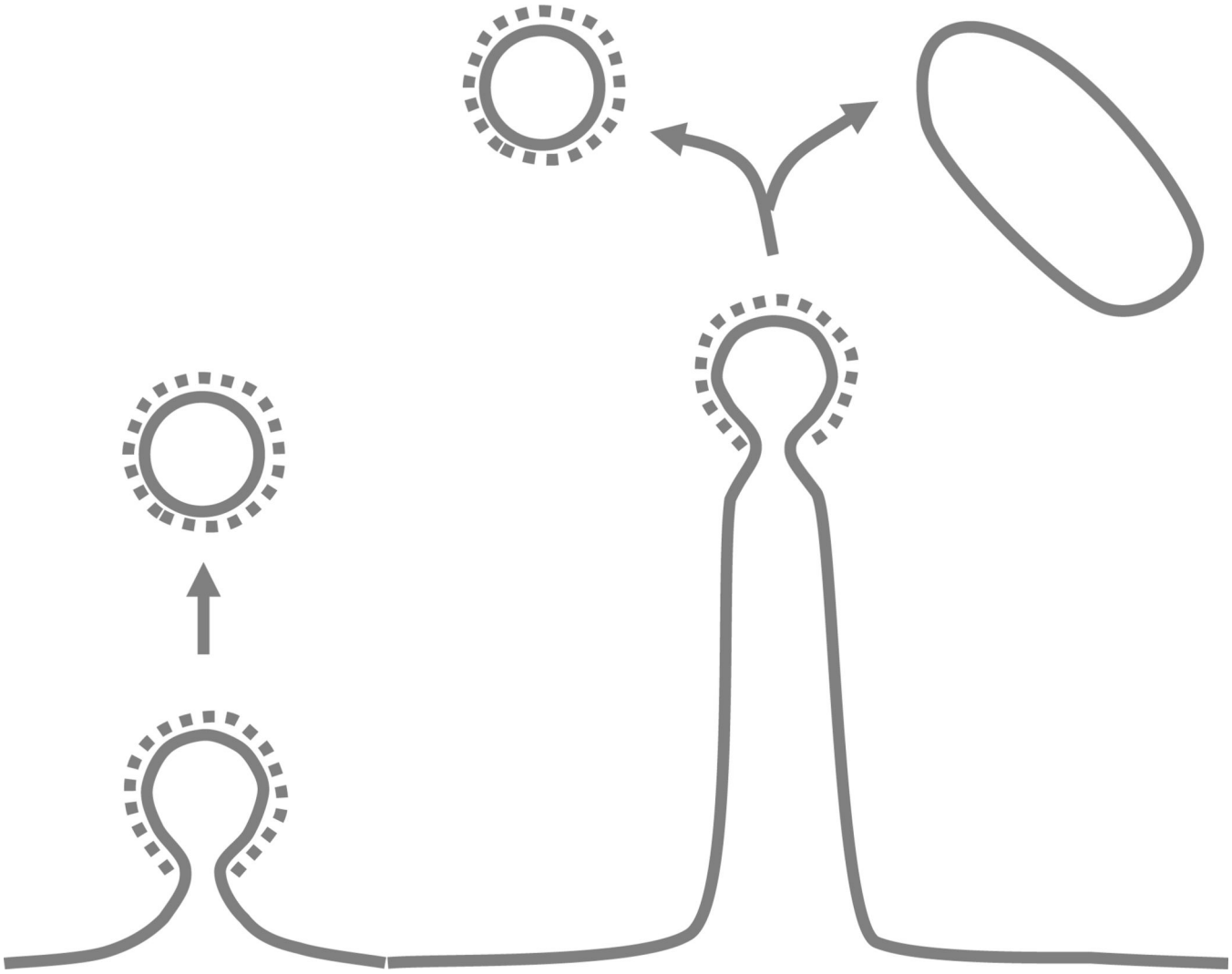

Figure 5.

Schematic representation of the membrane invaginations described in this study and of their fission. The model illustrates how an endocytic reaction triggered by clathrin may lead to both classical clathrin-coated vesicles derived from the coated bud and non-coated larger vesicles derived from the tubular region.